frontiers | Frontiers in Biomaterials Science

TYPE Original Research
PUBLISHED 25 June 2024
DOI 10.3389/fbiom.2024.1362599

OPEN ACCESS

EDITED BY
Jenny Robinson,
University of Washington, United States

REVIEWED BY
John Clegg,
University of Oklahoma, United States
Gemma Palazzolo,
Italian Institute of Technology (IIT), Italy
M. Tyler Nelson,
Wright-Patterson Air Force Base, United States

*CORRESPONDENCE
Chiara Tonda-Turo,
chiara.tondaturo@polito.it

†These authors have contributed equally to this work

RECEIVED 28 December 2023
ACCEPTED 06 June 2024
PUBLISHED 25 June 2024

CITATION
Licciardello M, Traldi C, Bortolameazzi M, Testore D, Ciardelli G and Tonda-Turo C (2024), Aligned polycaprolactone/polyaniline electrospun nanofibers for directing neural stem cell differentiation and neuron arrangement.
Front. Biomater. Sci. 3:1362599.
doi: 10.3389/fbiom.2024.1362599

Aligned polycaprolactone/polyaniline electrospun nanofibers for directing neural stem cell differentiation and neuron arrangement

Michela Licciardello[1,2,3†], Cecilia Traldi[1,2,3†], Matteo Bortolameazzi[1,2,3], Daniele Testore[1,2,3], Gianluca Ciardelli[1,2,3,4] and Chiara Tonda-Turo[1,2,3*]

[1]Department of Mechanical and Aerospace Engineering, La.Di.Spe Bioengineering, Politecnico di Torino, Turin, Italy, [2]POLITO BIOMedLAB, Politecnico di Torino, Turin, Italy, [3]Interuniversity Center for the Promotion of the 3Rs Principles in Teaching and Research, Pisa, Italy, [4]National Research Council-Institute for Chemical and Physical Processes (CNR-IPCF), Pisa, Italy

The use of engineered biomimetic substrates combined with neural stem cells (NSCs) constitutes a promising approach to develop reliable *in vitro* models of the nervous tissue. The fabrication of scaffolds with suitable compositional, topographical, and electrical properties is crucial for directing neural cell adhesion, differentiation, and arrangement. Herein, we propose the development of electroconductive polycaprolactone/polyaniline (PCL/PANI) electrospun mats as functional substrates for NSC culture. A rotating drum collector was employed to obtain fibers with aligned geometry. According to the results, the increase in alignment contributed to the reduction of fiber diameter and the increase of scaffold mechanical properties in terms of elastic modulus and tensile strength. *In vitro* experiments demonstrated the ability of PCL/PANI membranes to support NSC attachment and growth, as well as significantly foster neuronal differentiation. Furthermore, the presence of an aligned pattern was shown to effectively influence the arrangement of NSC-derived neurons, confirming the potential of this substrate for the design of a physiologically relevant culture platform for *in vitro* investigation of the nervous tissue.

KEYWORDS

electrospinning, electrical activity, topographical cue, ECM-like scaffolds, biomimetic substrates, *in vitro* nervous system modeling

1 Introduction

The nervous system is commonly considered one of the most complex systems in the human body. Due to its unique structural and functional characteristics, its pathophysiology is yet poorly understood, making the treatment of neurological disorders extremely challenging (Lu et al., 2022). Nervous tissue damage, caused by neurodegenerative conditions or traumatic injuries, often results in the progressive loss of neuronal cells and disruption of axonal bundles, leading to the interruption of nervous signal transmission below the injured segments. Indeed, the restoration of neuronal connectivity and the recovery of tissue functionality are significantly hampered by the

highly neurotoxic environment proper of chronic neurodegeneration and the poor regenerative potential of neurons, especially in the case of the central nervous system. Additionally, efficient clinical treatments are still lacking in this field, as existing therapies are limited to preventing secondary injury effects and are proving to be ineffective in curing neuronal dysfunction (Kaplan and Levenberg, 2022). Recently, neural tissue engineering has provided novel strategies for the *in vitro* modeling of the nervous system, contributing to the understanding of many mechanisms involved in neurological disorders, and the development of innovative regeneration approaches (Qiu et al., 2020). Indeed, the development of physiologically relevant *in vitro* systems is crucial for the identification of molecular pathways linked to tissue regeneration and holds great potential in drug screening. Therefore, significant efforts have been made by neural researchers to develop functional biomimetic platforms, able to recreate *in vitro* the distinctive properties of the nervous tissue (Rouleau et al., 2023). A wide range of biomaterials and biofabrication methods have been explored to replicate the native extracellular composition and structure and provide appropriate stimuli for directing neural cell behavior and maturation *in vitro*.

Among the numerous techniques exploited for the fabrication of bioengineered substrates (Babaliari et al., 2018; Cadena et al., 2021; Traldi et al., 2023), electrospinning technology has attracted considerable attention in neural tissue engineering and *in vitro* modeling, thanks to its ability to simply fabricate fibrous substrates resembling fiber-shaped cellular assemblies specific to nervous tissue structures (Hu et al., 2022). Electrospinning is a versatile technique that exploits the application of a high voltage between the needle of a syringe (containing the solution) and the collector plate (for the fiber deposition) (Isaac et al., 2021), to produce micro or nanofibrous substrates with a high surface-to-volume ratio and an interconnected porous structure. An appealing aspect of this approach is the possibility to obtain structures with different compositions, topography, and, consequently, properties by tuning the solution and process parameters (Giannitelli et al., 2018). Several studies have reported the use of electrospinning for the development of fibrous substrates that guide neural cell activity and nervous tissue regeneration, by providing several stimuli, such as biochemical (Cheong et al., 2019; Zhu et al., 2020), topographical (Gnavi et al., 2015b; 2015a; Karimi et al., 2018; Wu et al., 2020), or electrical (Zha et al., 2020; Zhang et al., 2021) cues.

Substrate conductivity is a key factor for electro-active tissue such as nervous tissue (Keshvardoostchokami et al., 2021). Indeed, electrical activity is a distinguishing feature of nervous tissue that can be exploited to guide tissue regeneration and enhance the biomimicry of tissue graft and *in vitro* models (Bierman-Duquette et al., 2022). Conductive polymers, such as poly (pyrrole) and PANI, have been used to confer electrical activity to nervous tissue-engineered scaffolds (Farkhondehnia et al., 2018; Zhao et al., 2018; Garrudo et al., 2019; Guo et al., 2023) thereby promoting neural cell differentiation and the formation of longer neurites (Jin and Li, 2015). In particular, PANI is widely selected for the preparation of electrospun scaffolds (Razak et al., 2015; Garrudo et al., 2019).

In the work of Garrudo et al. (2021), the author described the optimization of PANI and PCL ratio to obtain random nanofibers with ideal electroconductive properties and high biocompatibility for NSC culture.

However, due to its brittle nature and low processability, the blending of PANI with natural or synthetic polymers is required to obtain effective scaffolds for tissue engineering approaches (Palaniappan and John, 2008; Balint et al., 2014; Peidavosi et al., 2022). For instance, Peidavosi et al. (2022) reported the potential application of blending PANI with PCL and Barium Titanate to fabricate electrospun random mats as biocompatible substrates for bone cell culture.

In addition to electrical activity, the alignment of ECM and cells is a distinctive feature of nervous tissue (Chen et al., 2019). Then, many attempts have been made to produce scaffolds with an anisotropic pattern, intended to guide neural cell migration, differentiation, and out-growth by influencing the distribution of focal adhesion and the arrangement of actin filaments (Gnavi et al., 2015a; Kennedy et al., 2017; Ferraris et al., 2020; Hu et al., 2022). Electrospun substrates with aligned patterns have been successfully obtained by using different strategies (Jha et al., 2011; Amores de Sousa et al., 2020; Asheghali et al., 2020; Li et al., 2022). For instance, Amores de Sousa et al. (2020) produced aligned PCL nanofibers through a parallel plate-based collector to investigate the role of substrate morphology in directing NSC fate DSL. Differently, a touch-spun method was used in the work of Asheghali et al., who fabricated PCL nanofibrous mats with high control of fiber alignment, crystallinity, and diameter. The authors demonstrated the preferential orientation of NSCs according to the fiber main direction (Asheghali et al., 2020). Rotating drum collectors have been widely used to obtain aligned fibers through electrospinning technology, thanks to the possibility of tailoring scaffold properties by changing collection speed (Gnavi et al., 2015a; Zhu et al., 2015; Nitti et al., 2018; He et al., 2020). For example, Zhu et al. reported the fabrication of a highly aligned PCL electrospun substrate by using a rotating drum collector. Aligned fibers better promoted axonal growth and extension compared to random substrates (Zhu et al., 2015).

Furthermore, several groups demonstrated that the combination of electrical and topographical cues promotes and enhances neural cell growth and differentiation (Yang et al., 2016; Farkhondehnia et al., 2018; Qing et al., 2018; Eftekhari et al., 2020). As previously reported by Yang et al. (2016) the synergic effect of substrate anisotropy and conductivity enhanced the differentiation of rat pheochromocytoma PC12-L cells into neurons. Qing et al. (2018) fabricated an aligned electrospun silk mat functionalized with conductive reduced graphene paper that promoted neuronal differentiation of SH-SY5Y cells and the establishment of an interconnected neural network. In another work, Farkhondehnia et al. (2018) prepared aligned electrospun conductive nanofibers, composed of PANI/PCL/poly lactic-co-glycolic acid and explored the effect of topography and electrical stimulation on the proliferation and morphology of glioblastoma cells (A-172 cell line).

Recently, we described the preparation of biocompatible PCL/PANI electrospun mats as a promising substrate for tissue engineering applications (Licciardello et al., 2021). Herein, we explored the potential of PCL/PANI blend to obtain an electroconductive nanofibrous scaffold with aligned geometry by employing a rotating drum collector to mimic the anisotropic structure and electroactive properties of nervous tissue. The collector speed was optimized to obtain nanofibers with defect-free and highly oriented morphology. PCL/PANI nanofibrous membranes were characterized in terms of morphology, mechanical behavior, and wettability to evaluate the influence of

fiber alignment on scaffold physical properties. Then, we explored the feasibility of using PCL/PANI mats to establish a biomimetic neural cell culture system and create an optimal microenvironment for the growth and maturation of neural cells. In particular, we evaluate the effect of substrate composition and topography on NSC differentiation and arrangement. Indeed, *in vitro* experiments demonstrated that the fabricated scaffold effectively supports the growth and differentiation of NSCs in both neuronal and glial phenotypes recapitulating the *in vivo* multi-cellular composition. Immunofluorescence analysis underlined the ability of ECM-like nanofibrous mats to steer neuronal differentiation rather than standard 2D culture. In addition, when cultured on aligned PCL/PANI mats, the arrangement and neurite outgrowth of NSC-derived neurons were strongly influenced by the morphological cue of the substrate.

2 Materials and methods

2.1 Fabrication and characterization of PCL/PANI electrospun membranes

2.1.1 Formulation of solution

A PCL/PANI blended solution was formulated as previously described by authors (Licciardello et al., 2021). Briefly, 19 mg of (1S)-(+)-10-camphorsulfonic acid (CSA, 99%, Sigma Aldrich, Italy) were dispersed in 3 mL of 1,1,1,3,3,3-Hexafluoroisopropanol-d2 (HFP, 99% purity, Carlo Erba Reagents, Italy). After complete solubilization, 15 mg of PANI (emeraldine base, Mw = 100 kDa, Sigma Aldric, Italy) was added. The solution was sonicated for 3 min at 20 kHz and then stirred for 4 h, obtaining the PANI-doped solution (PANI:CSA). Meanwhile, a solution of PCL was prepared by dispersing 500 mg of PCL (Mn = 80 kDa, Sigma Aldrich, Italy) in 2 mL of HFP for 3 h under magnetic stirring. The PANI:CSA and PCL solution were mixed and left under stirring overnight, obtaining the PCL/PANI blended solution.

2.1.2 Evaluation of electroconductive properties of PCL/PANI

The conductivity of PCL/PANI blend was evaluated using a four-point probe instrument (Ossila, United Kingdom). The measurements were first performed on PCL/PANI films in a dry state to evaluate the effect of PANI on the electroconductive properties of PCL/PANI blend. Hence, PCL/PANI solution was evenly spread on a glass petri dish and left to dry overnight at room temperature (RT). In addition, a film of pure PCL was also prepared from a 10% w/v PCL solution in HFP. The conductivity of PCL/PANI electrospun nanofibers was measured in a wet state after incubating the membranes in deionized water overnight. The analysis was also conducted on electrospun PCL mats as controls. Before analysis, the obtained films and membranes were cut into small square specimens and their thickness (t) was measured through a digital caliber. The sheet resistance (R_s) was detected for each sample (n = 3 for each condition). Subsequently, resistivity (ρ) and conductivity (σ) of the samples were also calculated according to the following equations:

$$\rho = R_s{}^{*}t$$

$$\sigma = \frac{1}{\rho}$$

The conductivity values were reported as mean ± standard deviation (std dev).

2.1.3 Electrospinning of PCL/PANI membrane

The electrospun membranes were obtained using Novaspider instrument (CIC nanoGUNE, Spain) in vertical configuration, using the previously optimized parameters (20 kV voltage, 1,000 μL h^{-1} flow rate and 20 cm distance) (Licciardello et al., 2023). The electrospun fibers were collected on a plane collector or rotating drum, obtaining random (coded as PCL/PANI_RDN) or aligned (coded as PCL/PANI_ALG) fibers, respectively. To assess the influence of speed on fiber orientation and morphology, two drum speeds were tested: 800 rpm (coded as ALG_low speed) and 3,200 rpm (ALG_high speed). After fabrication, the resulting membranes were dried overnight at RT.

2.1.4 Scanning electron microscopy analysis (SEM)

The morphological features of PCL/PANI_RDN and PCL/PANI_ALG electrospun mats were investigated through scanning electron microscopy (SEM, Tescan Vega). Before analysis, all the samples were cut into 1 cm^2 pieces and coated with a thin platinum layer using the sputtering instrument. ImageJ software was used to quantify the average diameter (n = 100 measurements for each sample). Moreover, the fiber alignment was evaluated by ImageJ Directionality plugin analyzing the orientation of both aligned and random fibers and quantifying the percentage of fibers oriented in the preferential direction.

2.1.5 Uniaxial tensile tests

The mechanical properties of membranes were evaluated using the uniaxial tensile instruments MTS QTestTM/10 equipped with a fixed lower crossbar and an upper mobile crossbar. Before tests, the samples were cut in dog-bone shape and then mounted between the grips of the instruments. The samples (n = 3 samples for each membrane type) were tested at a displacement of 2 mm/min using a 10 N load cell. The stress-strain curves of PCL/PANI_RND and PCL/PANI_ALG samples were plotted and used to calculate Young's modulus (E), ultimate tensile strength (UTS) and strain at failure (ε %).

2.1.6 Transwell insert modification

Transwell inserts (CellQART®, SABEU GmbH & Co. KG, Germany) were modified to lodge the electrospun mats, as previously described (Licciardello et al., 2023). Briefly, the poly (ethylene terephthalate) (PET) membranes were removed from the inserts. Sylgard 184 Polydimethylsiloxane base (PDMS, VWR) and the curing agent were mixed in a ratio of 10:1 wt./wt obtaining a viscous PDMS solution. A thin layer of PDMS was applied on the outer walls of the plastic inserts and a first incubation was performed at 90°C for 10 min to allow a pre-curing of PDMS. The PCL/PANI_RND and PCL/PANI_ALG mats were cut into 3 cm × 3 cm pieces and then positioned on the support. The complete crosslinking of PDMS was promoted by maintaining

the inserts at 70°C for 2 min, thus obtaining the modified transwell systems (coded as PCL/PANI TWs).

2.1.7 Cold atmospheric plasma treatment

The electrospun mats were treated with the Argon cold atmospheric plasma process using Stylus Plasma Noble (Nadir S. r.l, Italy) under the previously optimized conditions (Licciardello et al., 2021): 10 kV_{pp} high voltage, 9 W of radiofrequency power and 7.5 slm argon flux. PCL/PANI TWs were positioned on the flat support of the instruments and then treated with plasma by manually moving the stylus on the apical and basolateral surfaces of the mats.

2.1.8 Water contact angle (WCA) measurement

The water contact angle of atmospheric plasma untreated and treated samples of electrospun membranes was evaluated using the Drop Shape Analyzer apparatus equipped with Advance software (Krüss Gmbh, Germany) for data acquisition. A drop of 2 µL of milliQ water was applied on the basolateral side of the PCL/PANI TWs and the WCA measurements (n = 3 for each sample) were recorded using the ellipse fitting method of the data acquisition software.

2.2 *In vitro* cell cultures

2.2.1 NSC culture on PCL/PANI electrospun membranes

Mouse NSCs (NE-4C, ATCC) were cultured in a growth medium composed of Eagle's Minimum Essential Medium (EMEM, ATCC), supplemented with 10% fetal bovine serum (FBS, Gibco) and 1% L-glutamine (L-Glu, Gibco). Cells were maintained at 37°C in a humidified atmosphere of 5% CO_2 on tissue culture flasks. Before NSC seeding, PCL/PANI TWs were subjected to atmospheric plasma treatment to enhance their wettability. Then, PCL/PANI TWs were sterilized through incubation in 2% antibiotic-antimycotic solution (Sigma Aldrich) overnight, followed by UV light irradiation for 1 h. NSCs were seeded at a density of 2×10^5 cells/cm^2 on the apical side of PCL/PANI TWs after conditioning the membranes with the growth medium for an hour. NE-4C cells (2×10^5 cells/cm^2) were also cultured on aligned PCL TWs and glass coverslips as controls. For NSC differentiation, cells were cultured in the growth medium for 3 days (until reaching 80%–90% of confluency), and then they were treated with a differentiation medium comprising the growth medium supplemented by 10^{-6} M retinoic acid (RA, Sigma Aldrich) for 4 days. The culture medium was changed every 2 days. NE-4C cells (2×10^5 cells/cm^2) were also cultured on glass coverslips as a control. CellTiter-Blue® assay was used to evaluate NSC viability on PCL/PANI electrospun membranes and to assess the influence of both cold atmospheric plasma treatment and fiber alignment on cell attachment and proliferation. Four different conditions were tested: cells seeded on untreated random membranes (RND_untreated), plasma-treated random membranes (RND_treated), untreated aligned membranes (ALG_untreated), and plasma-treated aligned membranes (ALG_treated). CellTiter-Blue® assay was performed at 1 day and 3 days of culture according to manufacturer protocol. Briefly, the culture medium was removed from PCL/PANI TWs (n = 3 for each condition) and samples were incubated in CellTiter-Blue® reagent solution (1:6 dilution in culture medium) at 37°C for 1 h. Fluorescence intensity values were recorded by using SYNERGYTM HTX multimode plate reader (BioTeK, Winooski, VM, United States) with a 530 nm excitation/590 nm emission filter set.

2.2.2 Fluorescence and immunofluorescence staining

Fluorescence staining of cell nuclei and cytoskeletons was performed on NSCs seeded on random (RND) and aligned (ALG) membranes after 3 days of culture. This test was performed to analyze NSC behavior on untreated and plasma-treated mats and qualitatively attest the cell confluency required before starting cell differentiation. For cell fixing, PCL/PANI TWs were rinsed with PBS, and incubated in paraformaldehyde 4% in PBS (PFA, Alfa Aesar) at RT. After 30 min, samples were washed twice with PBS and permeabilized with 0.5% v/v Triton X-100 solution in PBS for 10 min. Then, Flash Phalloidin Green 488 (Phalloidin, BioLegend) was added to the apical compartment of PCL/PANI TWs as 1:60 diluted solution in 1% v/v bovine serum albumin (BSA, Sigma Aldrich) in PBS and incubated for 40 min at RT, avoiding exposure to light. Lastly, 4′,6-Diamidino-2-Phenylindole, Dihydrochloride (DAPI, Invitrogen) was used to stain nuclei by incubation in 1:1,000 DAPI solution in PBS in the dark for 10 min.

For NSC differentiation, NE-4C cells were cultured on RND and ALG membranes for up to 14 days after RA induction. Immunofluorescence staining was carried out to investigate the expression of neuron- and astrocyte-specific markers on days 0, 7, and 14 from RA induction. PCL/PANI TWs were fixed with PFA 4% in PBS for 40 min at RT and permeabilized with 0.2% v/v Triton X-100 solution in PBS for 10 min. 2% BSA solution in PBS was used as blocking buffer and incubated for 1 h at RT. Later, primary antibody (Table 1) solutions (diluted in PBS with 1% v/v BSA and 0.1% v/v Tween 20) were added to the apical compartment of PCL/PANI TWs and maintained at 4°C overnight. After washing with 1% v/v BSA and 0.1% v/v Tween 20 solution in PBS, samples were incubated in secondary antibody solutions (Table 1) at RT for 1 h. Then, samples were rinsed with PBS and cell nuclei were stained with DAPI as detailed above.

Before the imaging, the PCL/PANI membranes were separated from the TW inserts and mounted on glass coverslips by using Fluoromount™ Aqueous Mounting Medium (Sigma Aldrich). All images were acquired with the Eclipse Ti2 confocal microscope (Nikon). ImageJ software and the Directionality plugin were used for image analysis. The expression levels of differentiation markers were evaluated and reported as mean ± std dev of the fluorescence intensity of MAP2 and GFAP-related signals for NSC-derived neurons and astrocytes, respectively. In addition, the percentages of neuronal and astroglial cells were calculated considering MAP2 and GFAP stain-positive areas. Lastly, the assessment of neuron cytoskeleton orientation on aligned nanofibers was conducted by processing MAP2 images for NSC-derived neurons. Specifically, the alignment level of neurons was calculated as the difference in degrees between the main orientation angles of nanofibers and neurofilaments, obtained by Fourier spectrum analysis. For each experimental condition (n = 3), three image fields of each sample were considered.

TABLE 1 List of primary and secondary antibodies used for neural cell labeling in immunofluorescence staining.

Antibody	IgG subclass	Source	Dilution
Primary mouse anti-MAP2 (clone AP20)	IgG	Sigma Aldrich	1:500
Primary rabbit anti-GFAP (Polyclonal)	—	Agilent	1:500
Secondary Alexa Fluor 488 goat anti-mouse	IgG (H + L)	Invitrogen	1:1,000
Secondary Alexa Fluor 555 goat anti-rabbit	IgG (H + L)	Invitrogen	1:500

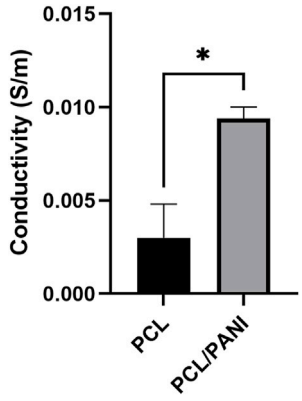

FIGURE 1
Analysis of the electroconductive properties of PCL/PANI electrospun membrane. Comparison of the conductivity values detected for PCL/PANI mats (PCL/PANI) and pure PCL mats (PCL) in wet conditions. Data are presented as mean ± std dev (n = 3). Statistical difference (*p < 0.1).

2.3 Statistical analysis

Statistical analyses were performed using GraphPad software (San Diego, CA, United States). A t-test analysis was used to evaluate differences in electroconductivity analysis, membrane mechanical properties, and cell alignment over time. A one-way ANOVA was conducted to record statistical differences in mat morphological properties and neural cell differentiation, while a two-way ANOVA was performed for the analysis of data from WCA, cell viability on the different substrates, and neural marker relative expressions.

3 Results

3.1 Electroconductive properties of PCL/PANI

The effect of PANI on the electroconductive properties of PCL/PANI was evaluated through the four-point probe method. According to the results, the PCL/PANI blend displayed a conductivity of 66 ± 15 S/m. As expected, the conductivity of pristine PCL was found to be undetectable due to the non-conductive nature of the material. Moreover, the electroconductive properties of PCL/PANI nanofibers were measured in wet conditions following overnight incubation in deionized water. As shown in Figure 1, the detected conductivity value of PCL/PANI mats was 0.009 ± 0.001 S/m. This value was significantly higher compared to PCL mats, which display a conductivity of 0.003 ± 0.002 S/m (0.01). These results demonstrated the strong contribution of PANI in conferring electroconductive properties to the PCL/PANI membranes, creating electrically conductive domains on the substrate surface, useful for electrical signal transmission (Chen et al., 2013).

3.2 Morphological characterization of PCL/PANI membranes

The morphology and the arrangement of fibers were evaluated through SEM analysis. As shown in Figure 2, all the obtained mats presented a defect-free nanofibrous morphology. In particular, fibers collected onto the flat collector presented a random orientation with an average diameter of 355 ± 90 nm. Interestingly, fibers produced using a low speed (800 rpm) had no preferential orientation and an average diameter of 342 ± 50 nm while membranes generated using high speed (3,200 rpm) consisted of aligned fibers with an average diameter of 224 ± 53 nm (p < 0.0001). Indeed, according to the analysis of fiber distribution, the orientation of ALG_high speed (Figure 2F) fibers resulted to be more pronounced in a preferred direction rather than RND (Figure 2D) and ALG_low speed samples (Figure 2E). Moreover, as shown in Figure 2F, the amount of fibers oriented in the same direction was significantly higher in ALG_high speed mats (about 80%) than RND and ALG_low speed which instead displayed comparable values. In particular, the high variability of the amount values for RND and ALG_low speed could be attributed to the absence of preferential orientation of the fibers. According to these results, the high speed of 3,200 rpm was used to produce mats for further characterization.

3.3 Mechanical characterization of PCL/PANI membranes

The mechanical characterization of the electrospun mats was performed through uniaxial tensile test. Figure 3A shows the stress-strain curves of PCL/PANI_RND and PCL/PANI_ALG. Both the curves exhibited a near-linear elastic trend until the electrospun samples broke. As shown in the histograms, the UTS and E of aligned fibers were found to be higher than the random counterparts. In particular, E increased from 14.33 ± 1.81 MPa for the PCL/PANI_RND fibers to 35.06 ± 5.06 MPa for PCL/PANI_ALG fibers (p < 0.001). Moreover, the increase in fiber alignment led to an increase in UTS from 10.31 ± 0.56 MPa for PCL/PANI_RND to 17.73 ± 3.04 MPa for PCL/PANI_ALG (p <

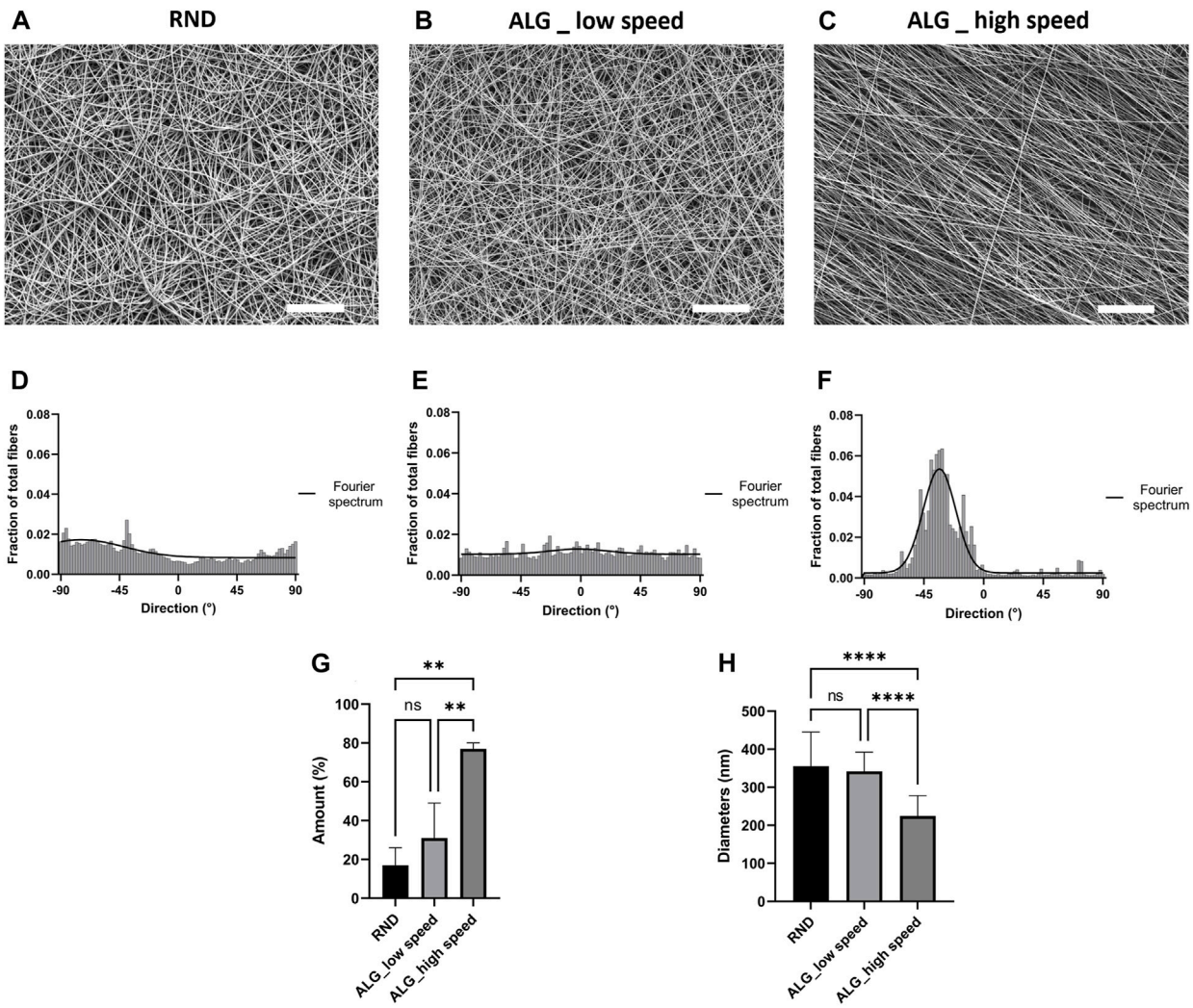

FIGURE 2
Morphological characterization of the electrospun membranes. **(A–C)** Representative SEM micrographs of RND **(A)**, ALG_low speed (800 rpm) **(B)** and ALG_high speed (3,200 rpm) **(C)** PCL/PANI nanofibers (scale bar = 20 μm). Quantification of fiber direction and Fourier spectrum of RND **(D)**, ALG_low speed (800 rpm) **(E)** and ALG_high speed (3,200 rpm) **(F)** PCL/PANI nanofibers. **(G)** Quantification of the amount of fibers oriented in the preferential direction. Data are presented as mean ± std dev (n = 3) **(H)** Comparison between RND, ALG_low speed and ALG_high speed fiber diameters Data are presented as mean ± std dev (n = 100). Statistical difference (**p < 0.01; ****p < 0.0001).

0.0001). Conversely, the ε% increased from 65.6 ± 8.2% for PCL/PANI_ALG fibers to 93.35% ± 11% for PCL/PANI_RND (p < 0.1).

3.4 Water contact angle and atmospheric plasma treatment of PCL/PANI membranes

The evaluation of the contact angle of the electrospun membranes was performed to investigate the influence of fiber topography and plasma treatment on the surface wettability of the electrospun mats. As shown in Figure 4, untreated PCL/PANI_RND and PCL/PANI_ALG displayed hydrophobic properties, presenting a water contact angle of 105.5° ± 6.6° and 119° ± 7.2° (p < 0.1), respectively. Thus, an atmospheric plasma treatment was performed to improve the surface wettability. The effective modification of the mat surface was confirmed by observing a reduction in water contact angle to 52.9° ± 19.3° and 76.3 ± 6.7 for PCL/PANI_RND (p < 0.0001) and PCL/PANI_ALG (p < 0.001), respectively. In addition, after plasma treatment, PCL/PANI_ALG presented higher mean values of water contact angles compared to PCL/PANI_RND, demonstrating that the topography slightly affects the surface properties of the substrate. In addition, a slight difference in WCA was detected between random and aligned samples, as the values of PCL/PANI_ALG were higher than PCL/PANI_RND, with a relevant statically difference after the plasma treatment.

3.5 NSC growth and viability on aligned PCL/PANI electrospun membranes

To validate the use of PCL/PANI electrospun membranes as culture substrates for neural cells, NE-4C cells were seeded on PCL/PANI TWs and cell viability was quantified after days 1 and 3 of

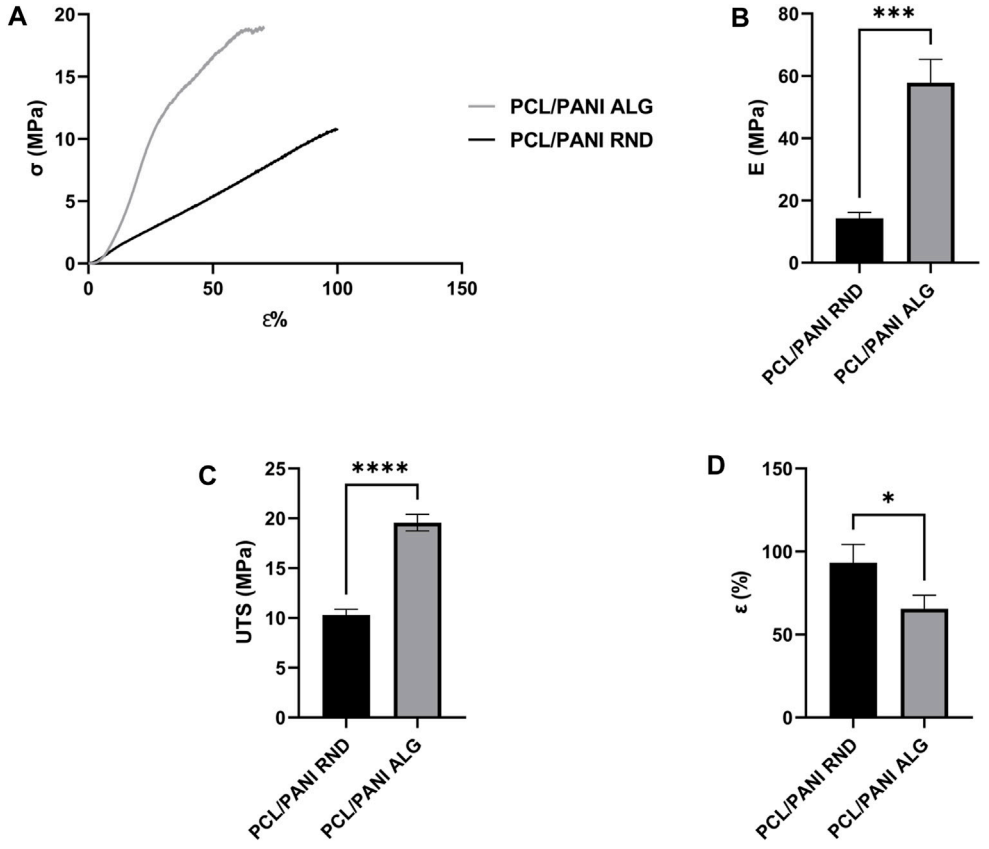

FIGURE 3
Mechanical characterization of the electrospun membranes. **(A)** Stress-strain curves of PCL/PANI_RND and PCL/PANI_ALG. Comparison between Young's modulus (E) **(B)**, ultimate tensile strength (UTS) **(C)** and strain at failure (ε %) **(D)**. Data are presented as mean ± std dev (n = 3). Statistical difference (*p < 0.1; ***p < 0.001 ****p < 0.0001).

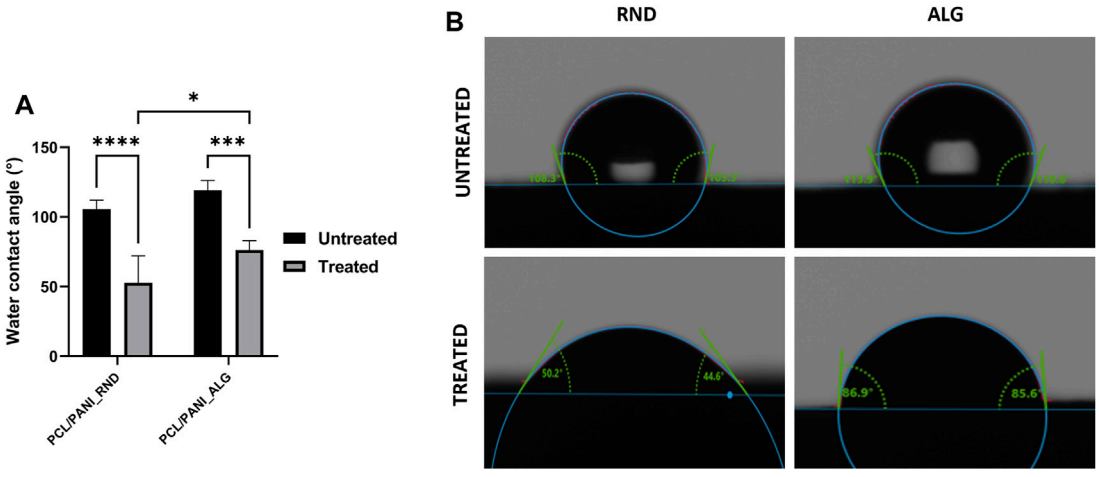

FIGURE 4
Characterization of surface wettability of the electrospun membranes. **(A)** Comparison of water contact angle values of RND and ALG mats before and after plasma treatment. **(B)** Representative contact angle images for droplets of water on RND and ALG mats before and after plasma treatment. Data are presented as mean ± std dev (n = 3). Statistical difference (*p < 0.1; ***p < 0.001 ****p < 0.0001).

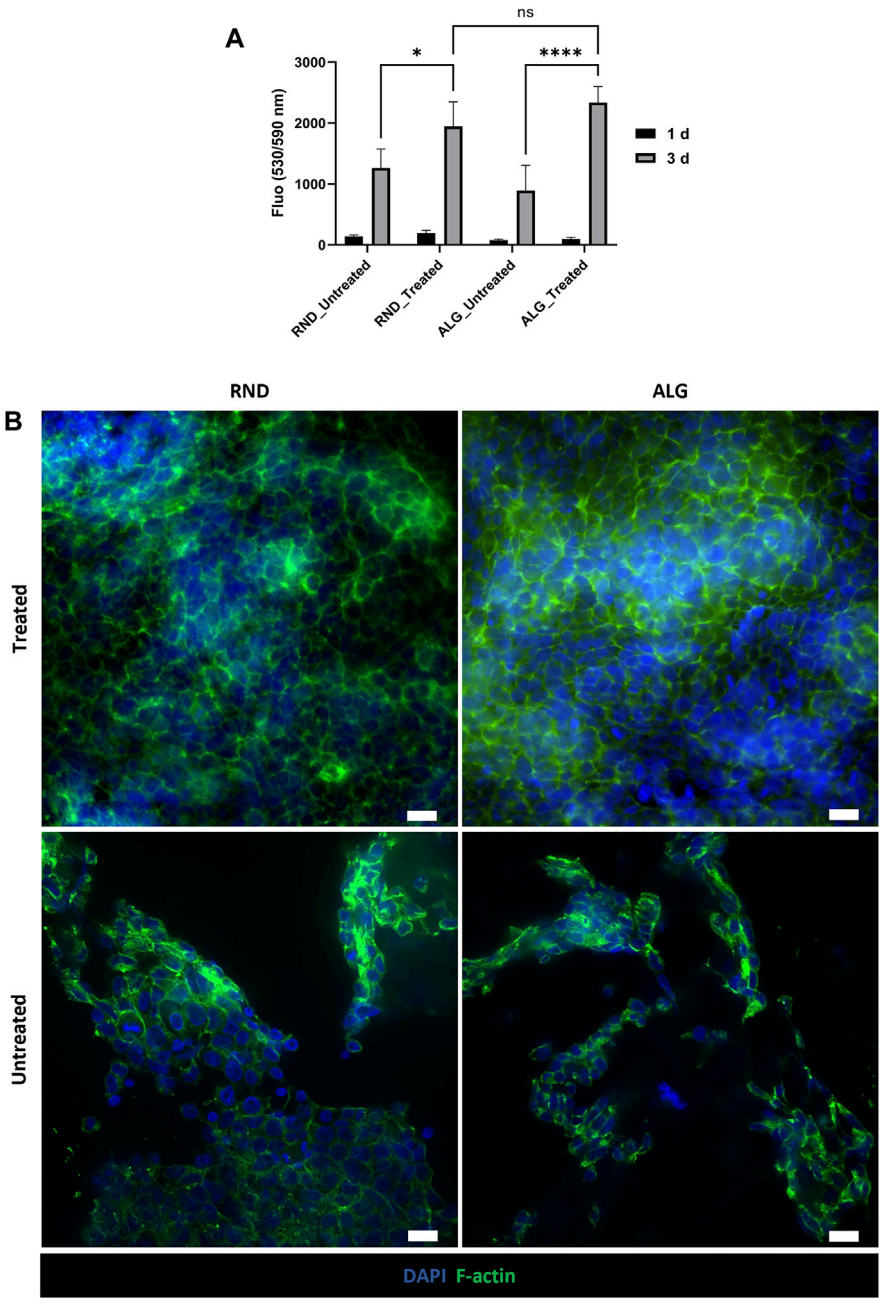

FIGURE 5
Evaluation of NSC behavior on PCL/PANI electrospun membranes. **(A)** Cell viability of NE-4C cells cultured on different substrates (plasma-treated or untreated, randomly oriented or aligned membranes). Data are presented as mean ± std dev (n = 3 biological replicates). Statistical difference (*p < 0.1; ****p < 0.0001). **(B)** Representative fluorescence images of cytoskeleton staining in NE-4C cell cultures on plasma-treated and untreated random and aligned membranes for 3 days (scale bar = 20 μm).

culture by using CellTiter-Blue® assay (Figure 5A). An increment in the recorded fluorescence values was detected after 3°days of culture in all the groups with slight differences among different samples, indicating cell proliferation over time. After 3°days, cell viability was significantly higher for cells seeded on plasma-treated membranes compared to untreated ones, while no statistically significant differences were observed between random and aligned fibrous membranes (Figure 5A). In addition, NSC morphology and distribution on plasma-treated and untreated membranes were evaluated by the fluorescence staining of cell nuclei and actin filaments (Figure 5B). At 3°days of culture, NSCs formed a uniform monolayer on both random and aligned fibers, showing characteristic epithelial-like morphology. On the contrary, cells cultured on untreated mats displayed a different behavior, as they tended to agglomerate in separated clusters, suggesting a reduction of initial cell adhesion thus inducing the formation of aggregates over time. According to these results, plasma-treated PCL/PANI TWs were selected for the subsequent studies.

10.3389/fbiom.2024.1362599

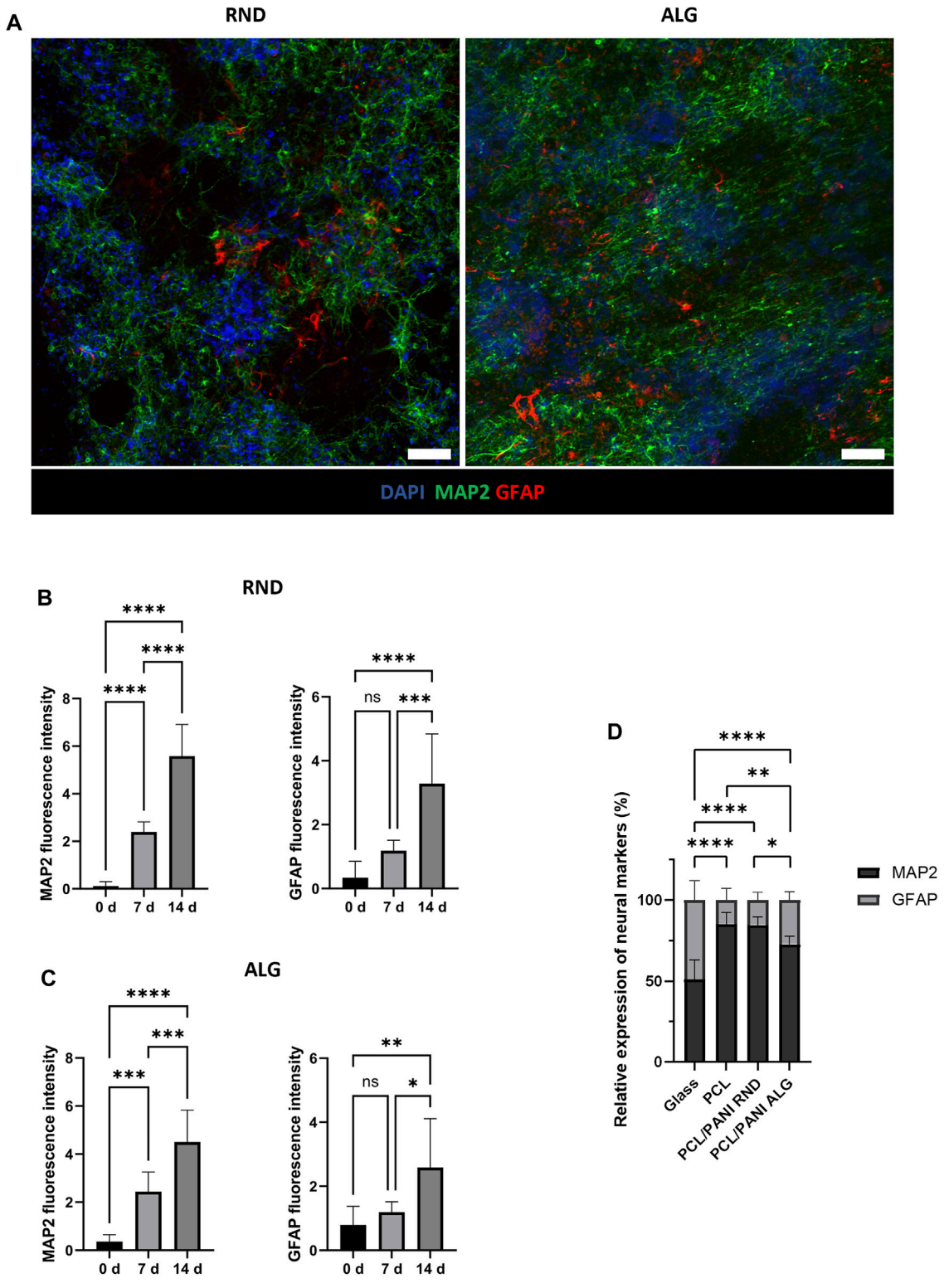

FIGURE 6
NSC differentiation on PCL/PANI electrospun membranes. **(A)** Representative immunofluorescence images for neuronal and astroglial markers in NE-4C cell cultures on both random (RND) and aligned (ALG) mats at 14°days after RA induction. Scale bar = 100 μm. **(B, C)** Expression levels of differentiation markers over time for NE-4C cells cultured on PCL/PANI random **(B)** and aligned **(C)** membranes. **(D)** Comparison of the percentages of MAP2 and GFAP stain-positive cells in NSC cultures on glass (Glass), aligned PCL mats (PCL), random PCL/PANI mats (PCL/PANI RND) and aligned PCL/PANI mats (PCL/PANI ALG) at 14°days after RA induction. Data are presented as mean ± std dev (n = 3 biological replicates; n = 3 technical replicates). Statistical difference (*p < 0.1; **p < 0.01; ***p < 0.001; ****p < 0.0001).

3.6 NSC differentiation on PCL/PANI electrospun membranes

The differentiation behavior of NSCs was evaluated by immunofluorescence analysis (Figure 6; Supplementary Figures S1, S2). The phenotypic characterization was conducted over 14°days after RA induction to assess the presence of different cell phenotypes and examine the effect of scaffold topography on NSC fate. Immunofluorescence staining revealed the presence of GFAP-expressing cells and MAP2-expressing cells after 14°days from RA induction, thus indicating NSC differentiation into astrocytes and mature neurons, respectively. In addition, MAP2-positive cells extended numerous neurites and interconnections all over the membranes (Figure 6A), suggesting high cell interaction with the substrate. It is noticed that MAP2 expression was upregulated already at 7°days compared to day 0 and it increased over the days, as confirmed by the greater fluorescence intensity (Figures 6B, C; Supplementary Figures S1, S2A). On the contrary, GFAP expression resulted to be not detectable at 0°days and 7°days, and GFAP-positive cells were stained only at 14°days (Figures 6B, C; Supplementary Figure S2B). Similar trends were observed in cells cultured on both aligned and random PCL/PANI TWs. For both the tested conditions, the number of MAP2-expressing cells was higher than GFAP ones, in contrast to cells seeded on glass. Indeed, the percentage of neurons exceeded over two times the percentage of astrocytes at 14°days, while it was quite comparable in the case of glass (Figure 6D; Supplementary Figure S3). NSCs cultured on PCL mats showed similar behavior, as no statistically significant differences were observed in the ratio of MAP2 to GFAP stain-positive cells between PCL fibers and random PCL/PANI fibers, while the ratio value was slightly higher compared to aligned PCL/PANI mats (Figure 6D; Supplementary Figure S3). Interestingly, the percentage of neurons was higher than that of astrocytes when NSCs were cultured on random PCL-PANI fibers (Figure 6D). Overall, these results revealed that PCL/PANI fibrous membranes can support NSC differentiation and promote the growth of mature neuron populations.

3.7 Influence of scaffold topography on neuronal cell alignment

The influence of fiber alignment on the behavior of neuronal cells was investigated by seeding NSCs on random and aligned PCL/PANI TWs. Differences in cell morphology and orientation were underlined by analyzing the arrangement of neuron-specific cytoskeletal protein on cells cultured in the two different conditions. According to the analysis of MAP2 staining, NSC-derived neurons exhibited directional neurite outgrowth along aligned fibers (Figures 7A, B, D), while they did not show a preferential orientation in the case of random membranes (Figure 7C). Indeed, the average difference between the orientation angles of MAP2-positive cells and aligned electrospun fibers was calculated to be around 11° at 7°days from RA induction (Supplementary Figure S4) and it is reduced by half in the late-stage differentiation (Figures 7D, E).

4 Discussion

Electrospun nanofibrous scaffolds have been extensively employed in nerve tissue engineering. Indeed, it is well known that the presence of topographical cues at the nanoscale level could play a pivotal role in influencing neural cell behavior, in terms of cell adhesion, proliferation, and maturation (Farrukh et al., 2018). On the other hand, electrical signals are crucial stimuli for electroactive tissue regeneration such as nerves (Rivers et al., 2002). Thus, the cell culture substrate should be specifically engineered to mediate electrical signaling between cells and respect the anisotropic structure of the native tissue.

In this work, an electroconductive substrate was obtained by blending PCL with PANI. To the best of our knowledge, electroconductive nanofibers have been obtained by using several synthetic polymers (alone or blended), however the use of electrospun aligned PCL/PANI nanofibers has not been reported for the fabrication of scaffolds for neural cell culture. Therefore, a detailed investigation of the effect of scaffold composition and anisotropy was conducted in this work, highlighting the contribution of the different substrate properties on guiding NSC fate.

Firstly, the analysis of surface conductivity on PCL/PANI films demonstrated that the presence of PANI conferred electroconductive properties to the PCL/PANI blend recording a conductivity of 66 ± 15 S/m. This value is in line with the conductivity achieved for PANI-based substrates as reviewed by Bierman-Duquette et al. (2022). Moreover, the inclusion of PANI into PCL nanofibers was shown to enhance the electroconductive properties of the electrospun membranes in wet conditions. PCL mats showed conductivity of 0.003 ± 0.002 S/m which is related to the presence of ions in the aqueous medium absorbed and retained by the nanofibrous substrate. The addition of the conductive dopant PANI in PCL/PANI nanofibers resulted in an overall increased conductivity (Figure 1), which is a combination of ionic-based conductivity of the absorbed medium and electron-based conductivity of the conductive polymer (Roshanbinfar et al., 2018). Indeed, PCL/PANI mats showed a conductivity of 0.009 ± 0.001 S/m which is in line with the values measured for PANI-based electrospun fibers reported in the literature (Garrudo et al., 2019, 2021).

Although previous studies evidenced that the combination of electrical and topographical features of the cell culture support can be an effective strategy to promote neural cell adhesion and neurite outgrowth, none of them have reported the ability of these substrates of modulating the co-differentiation of precursor cells in both neurons and astrocytes (Ghasemi-Mobarakeh et al., 2011). Anisotropic substrates have been shown to play a key role in providing topographical cues for neural cell body alignment along the fiber's axes (Wang et al., 2009; Badrossamay et al., 2014). To induce the fiber alignment, a drum collector was used during the electrospinning process. The influence of drum speed on fiber orientation was evaluated. In particular, the results of SEM analysis demonstrated that electrospun nanofibers became more aligned with increasing drum speed. Moreover, the Fourier spectrum analysis (Figure 2) revealed the presence of a sharper and higher peak of alignment for ALG_high speed mats compared to ALG_low speed that confirmed as the increase of collection speed

10.3389/fbiom.2024.1362599

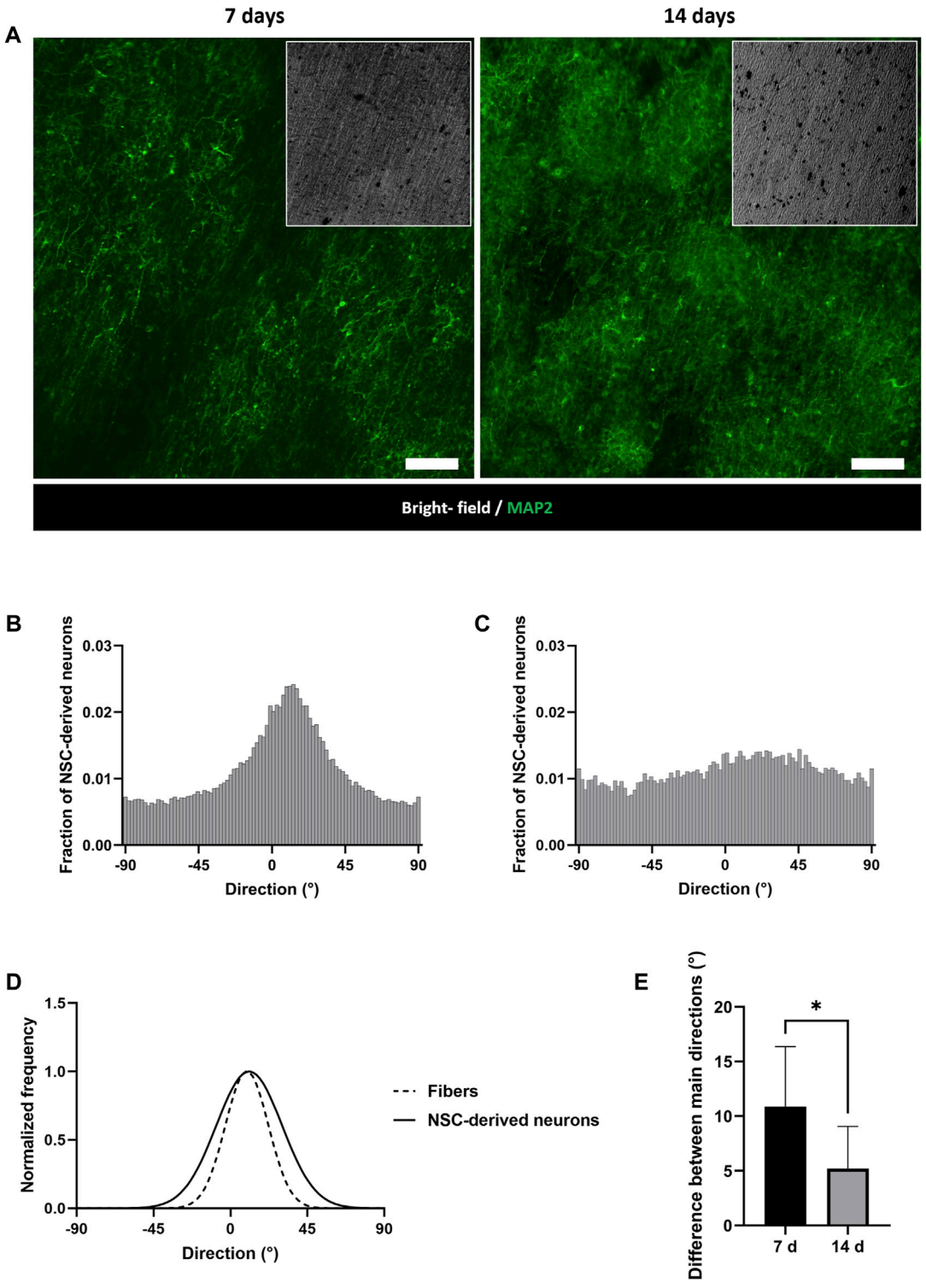

FIGURE 7
Evaluation of NSC-derived neuron orientation on PCL/PANI membranes. **(A)** Representative immunofluorescence images of MAP2-expressing cells on aligned mats at 7 and 14 days after RA induction. Scale bar = 100 μm. **(B, C)** Distribution of NSC-derived neuron directions on aligned **(B)** and random **(C)** PCL/PANI membranes at 14 days after RA induction. **(D)** Comparison between the main directions of NSC-derived neurons and fibers at 14 days after RA induction by Fourier spectrum analysis. **(E)** Comparison between the alignment levels of NSC-derived neurons at 7 and 14 days. Data are presented as mean ± std dev (n = 3 biological replicates; n = 3 technical replicates). Statistical difference (*p < 0.1).

led to a higher percentage of nanofibers oriented in a preferential direction. These findings are in line with previous reports (Nitti et al., 2018; He et al., 2020). In particular, the improvement of fiber alignment was previously ascribed to the increase in the difference between the drum surface speed and the final fiber speed, which is enhanced in the case of high collection speeds (Sadrjahani et al., 2010). Based on our results, the optimal fiber alignment was achieved with a speed of 3,200 rpm, allowing for the fabrication of highly oriented nanofibrous mats. The uniaxial tensile test demonstrated that fiber alignment led to an enhancement of scaffold mechanical properties in terms of Young's modulus and tensile strength. Several studies have investigated the effect of fiber alignment on the mechanical properties of electrospun mats, demonstrating that nanofiber orientation towards a preferential direction can lead to increased tensile strength and Young's modulus in electrospun mats (El-hadi and Al-Jabri, 2016; Merighi et al., 2019; Chen et al., 2021). Indeed, since the fiber orientation is in the direction of the load, the fiber's uniaxial orientation allows for the equal distribution of the tensile force to all fibers. Thus, the increase in tensile strength and Young's modulus was ascribed to the orientation of the molecular chains in the axis of the fiber. In particular, when aligned fibers are obtained through a rotating collector, its rotational speed leads to the application of mechanical forces to the polymeric jet, thus inducing the stretching of the polymer chains along the fiber axis. In addition, the morphological analysis highlighted a correlation between the fiber diameter and the drum speed, revealing that the fiber diameter decreased as the collector speed increased due to the higher stretching level imposed on fibers during the drum rotation (Medeiros et al., 2008). Several studies reported the correlation between fiber diameter and mechanical properties of the electrospun mats (Baji et al., 2010). The electrospun mats presented thinner diameters at higher collection speeds, leading to an increase in the membrane's strength (Shin et al., 2006; Pai et al., 2011; Yao et al., 2014; Pham et al., 2021). The surface properties of PCL/PANI membranes were improved by treating electrospun mats with atmospheric argon plasma. Indeed, PCL/PANI mats were found to be highly hydrophobic, displaying a contact angle higher than 100° regardless of fiber orientation. After plasma exposure, the detected values of wettability decreased to around 53° and 76°, for random and aligned fibers, respectively (Figure 4). The argon plasma treatment causes the formation of polar groups on fiber surfaces, allowing water to more easily enter the scaffold pores (Ivanova et al., 2018; Miroshnichenko et al., 2019; Licciardello et al., 2021). Additionally, the WCA was slightly higher in the case of aligned fibers, suggesting that fiber morphology also influences the wettability of PCL/PANI mats. Indeed, the presence of an aligned pattern results in changes in mat porosity and fiber diameter and consequently in the surface properties of the membranes. By comparing the results of the morphological analysis between random and aligned membranes, a reduction of fiber diameter was found with the increased level of alignment. These findings are consistent with the investigation of Sivan et al., who suggested that the value of the contact angle of PCL nanofibrous mats is inversely proportional to the diameter of the fibers, as it determines the extent of the contact area (Sivan et al., 2020).

The influence of scaffold anisotropy on cell viability and differentiation has been investigated *in vitro* using PCL/PANI membranes as culture substrates for neural cells. NSCs were successfully cultured on the electroconductive nanofibrous mats and differentiated into mature neuronal and astroglial cells. Viability analysis and fluorescence staining demonstrated that PCL/PANI membranes are able to support NSC attachment and growth, as confirmed by the formation of a confluent cell monolayer within 3 days of seeding (Figure 5B). A significant increase of viable cells was detected in the case of plasma-treated samples, confirming that the surface modification can improve scaffold hydrophilicity and then cell adhesion, reducing the formation of cell aggregates (Figures 5A, B). Indeed, it has been reported that surface wettability considerably affects the absorption and conformation of proteins from the culture medium, which subsequently mediate cell binding (Cai et al., 2020). Beyond scaffold surface properties, many other features such as scaffold topography and alignment are known to influence cell attachment and outgrowth. However, no significant differences have been noticed between random and aligned fibers in terms of NSC viability, as comparable values of fluorescence were reached at 3°days (Figure 5A). Additionally, the cell nuclei and F-actin staining did not show any changes in cell morphology and cytoskeleton arrangement according to fiber orientation (Figure 5B). It is reported in the literature that the effect of fiber alignment is strictly correlated with fiber diameters. Indeed, fibers displaying average diameters lower than around 700 nm were shown to promote the proliferation of NSCs, by forming uniform mats and minimizing the effects of topography in growth conditions (Christopherson et al., 2009; Garrudo et al., 2019). Accordingly, the calculated fiber diameters in our work were 224 ± 53 nm and 355 ± 90 nm, for aligned and random fibers, respectively, which are both included in the range cited above. These results suggest that plasma-treated PCL/PANI mats can support neural cell adhesion and growth without affecting their stemness state, as confirmed by the maintenance of NSC proper morphology and highly proliferative behavior.

Secondly, the differentiation of NSCs was performed by culturing them on PCL/PANI electrospun membranes to investigate the influence of scaffold anisotropy on NSC fate and maturation. NE-4C cells are known to have the capability of differentiating into neurons and astrocytes under RA treatment (Schlett and Madarász, 1997). After 14°days after RA induction, cells seeded on both random and aligned fibers expressed neuronal and astroglial markers and created interconnected neural networks on the entire membrane (Supplementary Figure S5; Supplementary Video S1). By analyzing the time course of marker expressions, the formation of neural aggregates displaying neuron characteristics was observed on day 7 after RA induction, while GFAP-expressing astrocytes appeared at 14°days (Figure 6; Supplementary Figure S2). This is in line with NE-4C neurogenesis stages described in the literature, where the onset of astroglia cells follows the main neuronal differentiation. Indeed, different studies reported that GFAP-positive cells were noted not sooner than the ninth day of RA treatment (Schlett and Madarász, 1997; Varga et al., 2008; Hádinger et al., 2009). Moreover, according to immunofluorescence images, the morphology and arrangement of differentiated NE-4C cells respected the characteristics reported in the literature, as interconnected neuronal aggregates were observed on a cell monolayer, while astrocytes were located inside and around the clusters (Figure 6A) (Varga et al., 2008). In addition, marker

stain-positive areas were calculated to estimate the number of cells undergoing neuronal and glial differentiations. According to the analysis, the percentage of cells expressing MAP2 was significantly higher than GFAP-labeled cells, confirming that NSCs preferentially differentiate into neurons on PCL/PANI mats. Indeed, neuronal cells resulted to be more than 70% of cells expressing neural markers, either in the case of random or aligned mats (Figure 6D). The same trend was also observed in cells cultured on PCL mats. Differently, the number of neurons and astrocytes was comparable when NE-4C cells were seeded on glass. In general, these results suggest that fiber-based substrates promoted neuronal differentiation, providing a biomimetic environment for neural cells. Indeed, although the values of Young's modulus in PCL-PANI mats are significantly higher than that of brain tissue, whose elastic modulus ranges from 0.1 to 1 kPa (Tarricone et al., 2022), they can be considered more similar to the one of native tissue compared to glass (~GPa) (Ford and Rajagopalan, 2018).

Interestingly, the ratio of neurons to astrocytes was higher for PCL/PANI random mats than aligned ones (Figure 6D). This aspect is apparently in contrast to what was reported in the work of Ashegali and colleagues, who showed a correlation between higher alignment and increased ratio of TUJ1-labeled neurons to GFAP-labeled astrocytes (Asheghali et al., 2020). Several studies underlined the importance of anisotropy in enhancing neuronal differentiation (Lim et al., 2010; Mohtaram et al., 2015; Eftekhari et al., 2020). However, it is well-documented that the mechanical properties of scaffolds are equally important in directing NSC fate (Farrukh et al., 2018). It is reported that NSCs preferentially differentiate into neurons on substrates having low elastic modulus while stiffer materials induce their differentiation into astrocytes (Saha et al., 2008; Ali et al., 2015). In this work, a higher percentage of astrocytes was detected on aligned fibers, which presented both a biomimetic aligned orientation and enhanced mechanical properties in terms of Young's modulus and tensile strength compared to random counterparts. Accordingly, the GFAP stain-positive area was higher in the case of NSC culture on glass, as cells were differentiated on stiff substrates (~GPa) (Ford and Rajagopalan, 2018). In summary, the capability of PCL/PANI nanofibrous mats in boosting the differentiation of cultured NSCs into neurons was demonstrated, in contrast to traditional over differentiation in glial cells, also evidencing the possibility of modulating the ratio between the two cell populations depending on substrate physical properties.

Lastly, the use of PCL/PANI mats in modulating neuron arrangement and neurite outgrowth was assessed. Several studies have shown the potential of aligned structures in directing neurite extension (Wang et al., 2009; Mohtaram et al., 2015; Hyysalo et al., 2017; Amores de Sousa et al., 2020). This aspect has been proven to be a very important factor for regulating *in vitro* neuronal activity (Hajiali et al., 2018) and significantly contributes to the maturation of *in vitro* neural tissues, especially in combination with exogenous electrical stimulation (Eftekhari et al., 2020). In our study, the effect of aligned fiber configuration was investigated on NSC-derived neurons. Specifically, neuronal morphology was evaluated by analyzing the localization of cytoskeleton protein with respect to fiber orientations. According to immunofluorescence imaging, cells cultured on aligned mats were arranged in a preferential direction, following fiber main orientation angles (Figures 7A, D). Indeed, by comparing the Fourier spectra of angle distributions, a difference lower than 5° was observed between the primary directions of neurons and fibers at 14°days (Figure 7E). On the contrary, a wide distribution was found in the case of neurons seeded on random mats, where no trend in cell orientation can be identified (Figure 7C). These results confirmed that the presence of aligned patterns in the PCL/PANI nanofibrous mats directly influenced neuronal cell spreading and neurite attachment and could provide contact guidance for axonal elongation towards a preferential direction.

5 Conclusion

In this work, the use of electroconductive PCL/PANI nanofibrous membranes was proposed to develop functional scaffolds for neural stem cell culture and nervous tissue modeling. The electrospinning process was employed to fabricate nanofibers in both random and aligned configurations, to mimic the typical nanofibrous and anisotropic architecture of the neural ECM. The interaction of NSCs with substrates having different physical and morphological properties was shown to stimulate specific cell responses in terms of cell differentiation and arrangement. The results of this work demonstrated that the nanofibrous structure of PCL/PANI mats significantly promoted the differentiation of NSCs into neurons compared to traditionally used glass substrates, supporting the establishment of an extended and interconnected neural network. Additionally, the presence of aligned patterns was proven to guide neuron orientation toward a preferential direction, providing biomimetic topographical cues for neurite outgrowth. The capability of this system to replicate some essential features of the *in vivo* microenvironment, such as tissue anisotropy and multi-cellular composition, makes it an attractive platform for the *in vitro* investigation of neuronal injuries and neurodegeneration, as well as the exploration of novel regenerative approaches. A step forward in model biomimicry would be the combined use of this platform with human induced pluripotent stem cell (hiPSCs) culture. Moreover, the electroactive properties of such nanofibrous substrates expand their applicability within dynamic systems for electrical stimulation or signal recordings, thus offering new opportunities for the creation of functional engineered tissue analogs.

Data availability statement

The original contributions presented in the study are included in the article/Supplementary Material, further inquiries can be directed to the corresponding author.

Author contributions

ML: Conceptualization, Data curation, Formal Analysis, Investigation, Methodology, Validation, Writing–original draft. CT: Conceptualization, Data curation, Formal Analysis, Investigation, Methodology, Validation, Writing–original draft. MB: Data curation, Investigation, Methodology, Writing–review and editing. DT: Methodology, Writing–review and editing. GC: Conceptualization, Funding acquisition, Resources, Writing–review

and editing. CT-T: Conceptualization, Data curation, Funding acquisition, Investigation, Methodology, Resources, Supervision, Writing–original draft, Writing–review and editing.

The author(s) declared that they were an editorial board member of Frontiers, at the time of submission. This had no impact on the peer review process and the final decision.

Funding

The author(s) declare that financial support was received for the research, authorship, and/or publication of this article. This project was carried out with the support of Fondazione Compagnia di San Paolo—Trapezio Call for Proposals-Target 1-project "Human multi-tissue platform for comprehensive evaluation of chemical toxicology on a chip."

Publisher's note

Conflict of interest

The authors declare that the research was conducted in the absence of any commercial or financial relationships that could be construed as a potential conflict of interest.

Supplementary material

The Supplementary Material for this article can be found online at: https://www.frontiersin.org/articles/10.3389/fbiom.2024.1362599/full#supplementary-material

References

Ali, S., Wall, I. B., Mason, C., Pelling, A. E., and Veraitch, F. S. (2015). The effect of Young's modulus on the neuronal differentiation of mouse embryonic stem cells. *Acta Biomater.* 25, 253–267. doi:10.1016/j.actbio.2015.07.008

Amores de Sousa, M. C., Rodrigues, C. A. V., Ferreira, I. A. F., Diogo, M. M., Linhardt, R. J., Cabral, J. M. S., et al. (2020). Functionalization of electrospun nanofibers and fiber alignment enhance neural stem cell proliferation and neuronal differentiation. *Front. Bioeng. Biotechnol.* 8, 580135–580216. doi:10.3389/fbioe.2020.580135

Asheghali, D., Lee, S. J., Furchner, A., Gruzd, A., Larson, S., Tokarev, A., et al. (2020). Enhanced neuronal differentiation of neural stem cells with mechanically enhanced touch-spun nanofibrous scaffolds. *Nanomedicine Nanotechnol. Biol. Med.* 24, 102152. doi:10.1016/j.nano.2020.102152

Babaliari, E., Kavatzikidou, P., Angelaki, D., Chaniotaki, L., Manousaki, A., Siakouli-Galanopoulou, A., et al. (2018). Engineering cell adhesion and orientation via ultrafast laser fabricated microstructured substrates. *Int. J. Mol. Sci.* 19, 2053. doi:10.3390/ijms19072053

Badrossamay, M. R., Balachandran, K., Capulli, A. K., Golecki, H. M., Agarwal, A., Goss, J. A., et al. (2014). Engineering hybrid polymer-protein super-aligned nanofibers via rotary jet spinning. *Biomaterials* 35, 3188–3197. doi:10.1016/j.biomaterials.2013.12.072

Baji, A., Mai, Y. W., Wong, S. C., Abtahi, M., and Chen, P. (2010). Electrospinning of polymer nanofibers: effects on oriented morphology, structures and tensile properties. *Compos. Sci. Technol.* 70, 703–718. doi:10.1016/j.compscitech.2010.01.010

Balint, R., Cassidy, N. J., and Cartmell, S. H. (2014). Conductive polymers: towards a smart biomaterial for tissue engineering. *Acta Biomater.* 10, 2341–2353. doi:10.1016/j.actbio.2014.02.015

Bierman-Duquette, R. D., Safarians, G., Huang, J., Rajput, B., Chen, J. Y., Wang, Z. Z., et al. (2022). Engineering tissues of the central nervous system: interfacing conductive biomaterials with neural stem/progenitor cells. *Adv. Healthc. Mater.* 11, 21015777–e2101628. doi:10.1002/adhm.202101577

Cadena, M., Ning, L., King, A., Hwang, B., Jin, L., Serpooshan, V., et al. (2021). 3D bioprinting of neural tissues. *Adv. Healthc. Mater.* 10, e2001600. doi:10.1002/adhm.202001600

Cai, S., Wu, C., Yang, W., Liang, W., Yu, H., and Liu, L. (2020). Recent advance in surface modification for regulating cell adhesion and behaviors. *Nanotechnol. Rev.* 9, 971–989. doi:10.1515/ntrev-2020-0076

Chen, C. H., Li, D. L., Chuang, A. D. C., Dash, B. S., and Chen, J. P. (2021). Tension stimulation of tenocytes in aligned hyaluronic acid/platelet-rich plasma-polycaprolactone core-sheath nanofiber membrane scaffold for tendon tissue engineering. *Int. J. Mol. Sci.* 22, 11215–11220. doi:10.3390/ijms222011215

Chen, M. C., Sun, Y. C., and Chen, Y. H. (2013). Electrically conductive nanofibers with highly oriented structures and their potential application in skeletal muscle tissue engineering. *Acta Biomater.* 9, 5562–5572. doi:10.1016/j.actbio.2012.10.024

Chen, Y., Taskin, M. B., Zhang, Z., Su, Y., Han, X., and Chen, M. (2019). Bioadhesive anisotropic nanogrooved microfibers directing three-dimensional neurite extension. *Biomater. Sci.* 7, 2165–2173. doi:10.1039/c8bm01603h

Cheong, H., Kim, J., Kim, B. J., Kim, E., Park, H. Y., Choi, B. H., et al. (2019). Multi-dimensional bioinspired tactics using an engineered mussel protein glue-based nanofiber conduit for accelerated functional nerve regeneration. *Acta Biomater.* 90, 87–99. doi:10.1016/j.actbio.2019.04.018

Christopherson, G. T., Song, H., and Mao, H. Q. (2009). The influence of fiber diameter of electrospun substrates on neural stem cell differentiation and proliferation. *Biomaterials* 30, 556–564. doi:10.1016/j.biomaterials.2008.10.004

Eftekhari, B. S., Eskandari, M., Janmey, P. A., Samadikuchaksaraei, A., and Gholipourmalekabadi, M. (2020). Surface topography and electrical signaling: single and synergistic effects on neural differentiation of stem cells. *Adv. Funct. Mater.* 30, 1–17. doi:10.1002/adfm.201907792

El-hadi, A. M., and Al-Jabri, F. Y. (2016). Influence of electrospinning parameters on fiber diameter and mechanical properties of poly(3-Hydroxybutyrate) (PHB) and polyanilines (PANI) blends. *Polym. (Basel)* 8, 97. doi:10.3390/polym8030097

Farkhondehnia, H., Amani Tehran, M., and Zamani, F. (2018). Fabrication of biocompatible PLGA/PCL/PANI nanofibrous scaffolds with electrical excitability. *Fibers Polym.* 19, 1813–1819. doi:10.1007/s12221-018-8265-1

Farrukh, A., Zhao, S., and del Campo, A. (2018). Microenvironments designed to support growth and function of neuronal cells. *Front. Mater.* 5, 1–22. doi:10.3389/fmats.2018.00062

Ferraris, S., Spriano, S., Scalia, A. C., Cochis, A., Rimondini, L., Cruz-Maya, I., et al. (2020). Topographical and biomechanical guidance of electrospun fibers for biomedical applications. *Polym. (Basel)* 12, 2896–2932. doi:10.3390/polym12122896

Ford, A. J., and Rajagopalan, P. (2018). Measuring cytoplasmic stiffness of fibroblasts as a function of location and substrate rigidity using atomic force microscopy. *ACS Biomater. Sci. Eng.* 4, 3974–3982. doi:10.1021/acsbiomaterials.8b01019

Garrudo, F. F. F., Chapman, C. A., Hoffman, P. R., Udangawa, R. W., Silva, J. C., Mikael, P. E., et al. (2019). Polyaniline-polycaprolactone blended nanofibers for neural cell culture. *Eur. Polym. J.* 117, 28–37. doi:10.1016/j.eurpolymj.2019.04.048

Garrudo, F. F. F., Mikael, P. E., Rodrigues, C. A. V., Udangawa, R. W., Paradiso, P., Chapman, C. A., et al. (2021). Polyaniline-polycaprolactone fibers for neural applications: electroconductivity enhanced by pseudo-doping. *Mater. Sci. Eng. C* 120, 111680. doi:10.1016/j.msec.2020.111680

Ghasemi-Mobarakeh, L., Prabhakaran, M. P., Morshed, M., Nasr-Esfahani, M. H., Baharvand, H., Kiani, S., et al. (2011). Application of conductive polymers, scaffolds and electrical stimulation for nerve tissue engineering. *J. Tissue Eng. Regen. Med.* 5, e17–e35. doi:10.1002/term.383

Giannitelli, S. M., Costantini, M., Basoli, F., Trombetta, M., and Rainer, A. (2018). "8 - electrospinning and microfluidics: an integrated approach for tissue engineering and cancer," in *Woodhead publishing series in biomaterials*. Editors V. Guarino and M. D. Ambrosio (Germany: Woodhead Publishing), 139–155. doi:10.1016/B978-0-08-101745-6.00008-6

Gnavi, S., Elena Fornasari, B., Tonda-Turo, C., Laurano, R., Zanetti, M., Ciardelli, G., et al. (2015a). The effect of electrospun gelatin fibers alignment on schwann cell and

axon behavior and organization in the perspective of artificial nerve design. *Int. J. Mol. Sci.* 16, 12925–12942. doi:10.3390/ijms160612925

Gnavi, S., Fornasari, B. E., Tonda-Turo, C., Ciardelli, G., Zanetti, M., Geuna, S., et al. (2015b). The influence of electrospun fibre size on Schwann cell behaviour and axonal outgrowth. *Mater. Sci. Eng. C* 48, 620–631. doi:10.1016/j.msec.2014.12.055

Guo, Y., Ghobeira, R., Aliakbarshirazi, S., Morent, R., and De Geyter, N. (2023). Polylactic acid/polyaniline nanofibers subjected to pre- and post-electrospinning plasma treatments for refined scaffold-based nerve tissue engineering applications. *Polym. (Basel)* 15, 72. doi:10.3390/polym15010072

Hádinger, N., Varga, B. V., Berzsenyi, S., Környei, Z., Madarász, E., and Herberth, B. (2009). Astroglia genesis *in vitro*: distinct effects of retinoic acid in different phases of neural stem cell differentiaion. *Int. J. Dev. Neurosci.* 27, 365–375. doi:10.1016/j.ijdevneu.2009.02.004

Hajiali, H., Contestabile, A., Mele, E., and Athanassiou, A. (2018). Influence of topography of nanofibrous scaffolds on functionality of engineered neural tissue. *J. Mater. Chem. B* 6, 930–939. doi:10.1039/c7tb02969a

He, H., Wang, Y., Farkas, B., Nagy, Z. K., and Molnar, K. (2020). Analysis and prediction of the diameter and orientation of AC electrospun nanofibers by response surface methodology. *Mater. Des.* 194, 108902–108909. doi:10.1016/j.matdes.2020.108902

Hu, Y., Zhang, H., Wei, H., Cheng, H., Cai, J., Chen, X., et al. (2022). Scaffolds with anisotropic structure for neural tissue engineering. *Eng. Regen.* 3, 154–162. doi:10.1016/j.engreg.2022.04.001

Hyysalo, A., Ristola, M., Joki, T., Honkanen, M., Vippola, M., and Narkilahti, S. (2017). Aligned poly(ε-caprolactone) nanofibers guide the orientation and migration of human pluripotent stem cell-derived neurons, astrocytes, and oligodendrocyte precursor cells *in vitro*. *Macromol. Biosci.* 17, 1–8. doi:10.1002/mabi.201600517

Isaac, B., Taylor, R. M., and Reifsnider, K. R. (2021). Mechanical and dielectric properties of aligned electrospun fibers. *Fibers* 9, 114–122. doi:10.3390/fib9010004

Ivanova, A. A., Syromotina, D. S., Shkarina, S. N., Shkarin, R., Cecilia, A., Weinhardt, V., et al. (2018). Effect of low-temperature plasma treatment of electrospun polycaprolactone fibrous scaffolds on calcium carbonate mineralisation. *RSC Adv.* 8, 39106–39114. doi:10.1039/c8ra07386d

Jha, B. S., Colello, R. J., Bowman, J. R., Sell, S. A., Lee, K. D., Bigbee, J. W., et al. (2011). Two pole air gap electrospinning: fabrication of highly aligned, three-dimensional scaffolds for nerve reconstruction. *Acta Biomater.* 7, 203–215. doi:10.1016/j.actbio.2010.08.004

Jin, G., and Li, K. (2015). The electrically conductive scaffold as the skeleton of stem cell niche in regenerative medicine. *Mater. Sci. Eng. C* 45, 671–681. doi:10.1016/j.msec.2014.06.004

Kaplan, B., and Levenberg, S. (2022). The role of biomaterials in peripheral nerve and spinal cord injury: a review. *Int. J. Mol. Sci.* 23, 1244. doi:10.3390/ijms23031244

Karimi, A., Karbasi, S., Razavi, S., and Zargar, E. (2018). Poly(hydroxybutyrate)/chitosan aligned electrospun scaffold as a novel substrate for nerve tissue engineering. *Adv. Biomed. Res.* 7, 44. doi:10.4103/abr.abr_277_16

Kennedy, K. M., Bhaw-Luximon, A., and Jhurry, D. (2017). Cell-matrix mechanical interaction in electrospun polymeric scaffolds for tissue engineering: implications for scaffold design and performance. *Acta Biomater.* 50, 41–55. doi:10.1016/j.actbio.2016.12.034

Keshvardoostchokami, M., Majidi, S. S., Huo, P., Ramachandran, R., Chen, M., and Liu, B. (2021). Electrospun nanofibers of natural and synthetic polymers as artificial extracellular matrix for tissue engineering. *Nanomaterials* 11, 21–23. doi:10.3390/nano11010021

Li, Y., Dong, T., Li, Z., Ni, S., Zhou, F., Alimi, O. A., et al. (2022). Review of advances in electrospinning-based strategies for spinal cord regeneration. *Mater. Today Chem.* 24, 100944. doi:10.1016/j.mtchem.2022.100944

Licciardello, M., Ciardelli, G., and Tonda-Turo, C. (2021). Biocompatible electrospun polycaprolactone-polyaniline scaffold treated with atmospheric plasma to improve hydrophilicity. *Bioengineering* 8, 24–18. doi:10.3390/bioengineering8020024

Licciardello, M., Sgarminato, V., Ciardelli, G., and Tonda-Turo, C. (2023). Development of biomimetic co-culture and tri-culture models to mimic the complex structure of the alveolar-capillary barrier. *Biomater. Adv.* 154, 213620. doi:10.1016/j.bioadv.2023.213620

Lim, S. H., Liu, X. Y., Song, H., Yarema, K. J., and Mao, H. Q. (2010). The effect of nanofiber-guided cell alignment on the preferential differentiation of neural stem cells. *Biomaterials* 31, 9031–9039. doi:10.1016/j.biomaterials.2010.08.021

Lu, D., Yang, Y., Zhang, P., Ma, Z., Li, W., Song, Y., et al. (2022). Development and application of three-dimensional bioprinting scaffold in the repair of spinal cord injury. *Tissue Eng. Regen. Med.* 19, 1113–1127. doi:10.1007/s13770-022-00465-1

Medeiros, E. S., Mattoso, L. H. C., Ito, E. N., Gregorski, K. S., Robertson, G. H., Offeman, R. D., et al. (2008). Electrospun nanofibers of poly(vinyl alcohol) reinforced with cellulose nanofibrils. *J. Biobased Mater. Bioenergy* 2, 231–242. doi:10.1166/jbmb.2008.411

Merighi, S., Mazzocchetti, L., Benelli, T., Maccaferri, E., Zucchelli, A., D'Amore, A., et al. (2019). A new wood surface flame-retardant based on poly-m-aramid electrospun nanofibers. *Polym. Eng. Sci.* 59, 2541–2549. doi:10.1002/pen.25235

Miroshnichenko, S., Timofeeva, V., Permykova, E., Ershov, S., Kiryukhantsev-Korneev, P., Dvořaková, E., et al. (2019). Plasma-coated polycaprolactone nanofibers with covalently bonded platelet-rich plasma enhance adhesion and growth of human fibroblasts. *Nanomaterials* 9, 637. doi:10.3390/nano9040637

Mohtaram, N. K., Ko, J., King, C., Sun, L., Muller, N., Jun, M. B. G., et al. (2015). Electrospun biomaterial scaffolds with varied topographies for neuronal differentiation of human-induced pluripotent stem cells. *J. Biomed. Mater. Res. - Part A* 103, 2591–2601. doi:10.1002/jbm.a.35392

Nitti, P., Gallo, N., Natta, L., Scalera, F., Palazzo, B., Sannino, A., et al. (2018). Influence of nanofiber orientation on morphological and mechanical properties of electrospun chitosan mats. *J. Healthc. Eng.* 2018, 1–12. doi:10.1155/2018/3651480

Pai, C. L., Boyce, M. C., and Rutledge, G. C. (2011). Mechanical properties of individual electrospun PA 6(3)T fibers and their variation with fiber diameter. *Polym. Guildf.* 52, 2295–2301. doi:10.1016/j.polymer.2011.03.041

Palaniappan, S., and John, A. (2008). Polyaniline materials by emulsion polymerization pathway. *Prog. Polym. Sci.* 33, 732–758. doi:10.1016/j.progpolymsci.2008.02.002

Peidavosi, N., Azami, M., Beheshtizadeh, N., and Ramazani Saadatabadi, A. (2022). Piezoelectric conductive electrospun nanocomposite PCL/Polyaniline/Barium Titanate scaffold for tissue engineering applications. *Sci. Rep.* 12, 20828–20913. doi:10.1038/s41598-022-25332-w

Pham, L. Q., Uspenskaya, M. V., Olekhnovich, R. O., and Baranov, M. A. (2021). The mechanical properties of PVC nanofiber mats obtained by electrospinning. *Fibers* 9, 1–12. doi:10.3390/fib9010002

Qing, H., Jin, G., Zhao, G., Huang, G., Ma, Y., Zhang, X., et al. (2018). Heterostructured silk-nanofiber-reduced graphene oxide composite scaffold for SH-SY5Y cell alignment and differentiation. *ACS Appl. Mater. Interfaces* 10, 39228–39237. doi:10.1021/acsami.8b12562

Qiu, B., Bessler, N., Figler, K., Buchholz, M. B., Rios, A. C., Malda, J., et al. (2020). Bioprinting neural systems to model central nervous system diseases. *Adv. Funct. Mater.* 30, 1910250. doi:10.1002/adfm.201910250

Razak, S. I. A., Wahab, I. F., Fadil, F., Dahli, F. N., Khudzari, A. Z., and Adeli, H. (2015). A review of electrospun conductive polyaniline based nanofiber composites and blends: processing features, applications, and future directions. *Adv. Mater. Sci. Eng.* 2015, 1–19. doi:10.1155/2015/356286

Rivers, T. J., Hudson, T. W., and Schmidt, C. E. (2002). Synthesis of a novel, biodegradable electrically conducting polymer for biomedical applications. *Adv. Funct. Mater.* 12, 33–37. doi:10.1002/1616-3028(20020101)12:1<33::AID-ADFM33>3.0.CO;2-E

Roshanbinfar, K., Vogt, L., Greber, B., Diecke, S., Boccaccini, A. R., Scheibel, T., et al. (2018). Electroconductive biohybrid hydrogel for enhanced maturation and beating properties of engineered cardiac tissues. *Adv. Funct. Mater.* 28. doi:10.1002/adfm.201803951

Rouleau, N., Murugan, N. J., and Kaplan, D. L. (2023). Functional bioengineered models of the central nervous system. *Nat. Rev. Bioeng.* 1, 252–270. doi:10.1038/s44222-023-00027-7

Sadrjahani, M., Hoseini, S. A., Mottaghitalab, V., and Haghi, A. K. (2010). Development and characterization of highly oriented pan nanofiber. *Braz. J. Chem. Eng.* 27, 583–589. doi:10.1590/S0104-66322010000400010

Saha, K., Keung, A. J., Irwin, E. F., Li, Y., Little, L., Schaffer, D. V., et al. (2008). Substrate modulus directs neural stem cell behavior. *Biophys. J.* 95, 4426–4438. doi:10.1529/biophysj.108.132217

Schlett, K., and Madarász, E. (1997). Retinoic acid induced neural differentiation in a neuroectodermal cell line immortalized by p53 deficiency. *J. Neurosci. Res.* 47, 405–415. doi:10.1002/(SICI)1097-4547(19970215)47:4<405::AID-JNR6>3.0.CO;2-I

Shin, M. K., Kim, S. I., Kim, S. J., Kim, S. K., Lee, H., and Spinks, G. M. (2006). Size-dependent elastic modulus of single electroactive polymer nanofibers. *Appl. Phys. Lett.* 89, 2004–2007. doi:10.1063/1.2402941

Sivan, M., Madheswaran, D., Asadian, M., Cools, P., Thukkaram, M., Van Der Voort, P., et al. (2020). Plasma treatment effects on bulk properties of polycaprolactone nanofibrous mats fabricated by uncommon AC electrospinning: a comparative study. *Surf. Coatings Technol.* 399, 126203. doi:10.1016/j.surfcoat.2020.126203

Tarricone, G., Carmagnola, I., and Chiono, V. (2022). Tissue-engineered models of the human brain: state-of-the-art analysis and challenges. *J. Funct. Biomater.* 13, 146. doi:10.3390/jfb13030146

Traldi, C., Chiappini, V., Menduti, G., Tonda-turo, C., and Boido, M. (2023). Advanced materials and biofabrication technologies to design *in vitro* functional central nervous system models. *Front. Med. Eng.* 1, 1–21. doi:10.3389/fmede.2023.1270943

Varga, B. V., Hádinger, N., Gócza, E., Dulberg, V., Demeter, K., Madarász, E., et al. (2008). Generation of diverse neuronal subtypes in cloned populations of stem-like cells. *BMC Dev. Biol.* 8, 89–18. doi:10.1186/1471-213X-8-89

Wang, H. B., Mullins, M. E., Cregg, J. M., Hurtado, A., Oudega, M., Trombley, M. T., et al. (2009). Creation of highly aligned electrospun poly-L-lactic acid fibers for nerve regeneration applications. *J. Neural Eng.* 6, 016001. doi:10.1088/1741-2560/6/1/016001

Wu, T., Xue, J., and Xia, Y. (2020). Engraving the surface of electrospun microfibers with nanoscale grooves promotes the outgrowth of neurites and the migration of schwann cells. *Angew. Chem.* 132, 15756–15762. doi:10.1002/ange.202002593

Yang, H., Zhu, G., Huang, Y., Shi, X., and Wang, Y. (2016). The stimulation of the differentiation of pheochromocytoma (PC12-L) cells into neuron-like cells by electrically conductive nanofibre mesh. *Appl. Mater. Today* 5, 215–222. doi:10.1016/j.apmt.2016.09.017

Yao, J., Bastiaansen, C. W. M., and Peijs, T. (2014). High strength and high modulus electrospun nanofibers. *Fibers* 2, 158–186. doi:10.3390/fib2020158

Zha, F., Chen, W., Hao, L., Wu, C., Lu, M., Zhang, L., et al. (2020). Electrospun cellulose-based conductive polymer nanofibrous mats: composite scaffolds and their influence on cell behavior with electrical stimulation for nerve tissue engineering. *Soft Matter* 16, 6591–6598. doi:10.1039/D0SM00593B

Zhang, J., Zhang, X., Wang, C., Li, F., Qiao, Z., Zeng, L., et al. (2021). Conductive composite fiber with optimized alignment guides neural regeneration under electrical stimulation. *Adv. Healthc. Mater.* 10, e2000604–e2000612. doi:10.1002/adhm.202000604

Zhao, Y. H., Niu, C. M., Shi, J. Q., Wang, Y. Y., Yang, Y. M., and Wang, H. B. (2018). Novel conductive polypyrrole/silk fibroin scaffold for neural tissue repair. *Neural Regen. Res.* 13, 1455–1464. doi:10.4103/1673-5374.235303

Zhu, L., Jia, S., Liu, T., Yan, L., Huang, D., Wang, Z., et al. (2020). Aligned PCL fiber conduits immobilized with nerve growth factor gradients enhance and direct sciatic nerve regeneration. *Adv. Funct. Mater.* 30. doi:10.1002/adfm.202002610

Zhu, W., Masood, F., O'Brien, J., and Zhang, L. G. (2015). Highly aligned nanocomposite scaffolds by electrospinning and electrospraying for neural tissue regeneration. *Nanomedicine Nanotechnol. Biol. Med.* 11, 693–704. doi:10.1016/j.nano.2014.12.001